

Vibrational properties of graphdiynes as 2D carbon materials beyond graphene

P. Serafini,^a A. Milani,^a M. Tommasini,^b C. Castiglioni,^b D.M. Proserpio,^{c,d} C.E. Bottani,^a C.S. Casari^{*a}

Two-dimensional (2D) hybrid sp-sp² carbon systems are an appealing subject for science and technology. For these materials, topology and structure significantly affect electronic and vibrational properties. We investigate here by periodic density-functional theory (DFT) calculations we here investigate the Raman and IR spectra of 2D carbon crystals belonging to the family of graphdiynes (GDYs) and having different structures and topologies. By joining DFT calculations with a symmetry analysis, we assign the IR and Raman modes in the spectra of all the investigated systems. On this basis we discuss how the modulation of the Raman and IR active bands depends on the different interactions between sp and sp² domains. The symmetry-based classification allows identifying the marker bands sensitive to the different peculiar topologies. These results show the effectiveness of vibrational spectroscopy for the characterization of new nanostructures, deepening the knowledge on the subtle interactions that take place in these 2D materials.

1 Introduction

In the last decades carbon materials and their nanostructures played an outstanding role in science and technology. Fullerenes, graphene, carbon nanotubes, and other carbon-based polyconjugated polymers are fundamental milestones that paved the way to the so-called “era of carbon allotropes”, enlightened by ground-breaking results and Nobel prizes [1].

In the last years, the interest has been directed toward novel forms of carbon, including 1D and 2D systems based on sp-hybridized carbon (variously referred to as carbyne, carbon atom wires, polyynes, cumulenes, ...) and on hybrid sp-sp² carbon systems. These investigations focused both on the fundamental properties and the potential applications in different fields, showing promising perspectives for the near future [2–6]. Graphyne (GY) and graphdiyne (GDY) represent 2D carbon crystals with sp-sp² carbon atoms [7–14]. They can be considered as a possible modification of graphene by interconnecting sp²-carbon hexagons with linear sp-carbon chains of different lengths (a single or a double acetylenic bond for GY and GDY, respectively), generating new systems with peculiar and tunable electronic and optical properties. Starting from GY and GDY and playing with geometry and topology, many other 2D hybrid sp-sp² carbon 2D systems can be proposed, offering countless possibilities in the design and tailoring of carbon allotropes both theoretically and experimentally. Early theoretical studies on GY- and GDY-based systems were reported in 1987 [15] and more recently modern computational methods have been employed to shed light on their properties [16–20].

These structures can be classified as covalent organic frameworks (COFs), showing the occurrence of Dirac cones, flat bands, and tunable bandgap [21,22]. Such features of the electronic structure of COFs have been explained based on

peculiar topological effects also in connection to their influence on the charge transport behaviour [23–26]. Several papers report on the prediction of properties of γ -GDY predicted mainly through density functional theory (DFT) calculations [5,6,27–32].

Vibrational spectroscopy turned out to be extremely useful to characterize carbon-based materials. Raman spectroscopy has been employed in the first experimental works reporting the preparation of GDY-based materials [33–37]. Despite the effectiveness of these spectroscopic techniques up to now and to our knowledge, only a few investigations focused on the prediction of the vibrational properties of GDY [35–37]. Popov et al. computed the Raman spectrum of different polymorphs of GY [34], Zhang et al. gave an assignment of the Raman spectrum of GY and GDY and studied the effects of strain by Raman [35]. Wang et al. discussed the Raman spectra of different finite-size models of different sp-sp² carbon nanostructures [37] while IR active C≡C stretching band has been discussed in Ref. [36]. In a previous paper, some of us carried out a detailed vibrational analysis of γ -GDY crystal and its nanoribbons, including a discussion of the associated Raman and IR spectra [31]. Nevertheless, it is still lacking an explorative vibrational analysis spanning across different graphdiynes, other than γ -GDY.

From the experimental side, synthetic bottom-up approaches have been successfully employed by Haley and co-workers [38–45] to produce sub-fragments of GDY of different topologies and dimension. Later, different papers reported the preparation and characterization of extended 2D GDY sheets prepared through organometallic synthesis techniques, showing promising routes to the production of these systems, even though significant efforts should still be put to further investigate and understand their properties [46–48]. Recent advances in on-surface synthesis allow the preparation of

hybrid $sp-sp^2$ carbon nanostructures and their atomic-scale investigation with surface science techniques [9,47,49–51]. Hence, the recent possibilities to realize new systems have opened new opportunities well beyond the sole investigation of their fundamental properties. In a previous paper, some of us developed an algorithm to systematically generate 2D carbon crystals belonging to the family of graphdiynes (GDYs) and having different structures and sp/sp^2 carbon ratios. We analyzed how structural and topological effects can tune the relative stability and the electronic behavior, to propose a rationale for the development of new systems with tailored properties [52].

Here, by using the set of 2D crystals generated in our previous work we investigate in detail the vibrational pattern of various graphdiyne systems. Two families of 2D materials have been considered. The first is composed of the simplest topologies of a single repeating unit, i.e. line (L), hexagon (H), and rhombus (R), and on widely studied polymorphs of GDY. The second family of 2D crystals (hereafter referred to as grazdynes, GZY) contains linear diacetylene chains (L) and extended sp^2 domains forming zig-zag sequences of CC bonds like polyacetylene and/or ribbons made by condensed aromatic rings with L chains linked to the zig-zag edges. For both groups of materials, we report an investigation of their vibrational structure, unveiling how different physicochemical effects can influence the vibrational spectra of GDY and GZY systems. For the first family (GDYs), the effect of topology and stability on the main Raman active bands is correlated to different structural features of the sp and sp^2 domains. At the same time, the IR spectra have been investigated to identify marker bands able to uniquely characterize the different 2D crystals. The same analysis extended to the second family shows how a different relative number of aromatic and L units affects the vibrational response of these materials. In these cases (GZYs), the Raman and IR spectra were investigated to correlate the crystal structure with the vibrational structure and π -conjugation effects. Our findings are relevant for the spectroscopic characterization of these materials, and may provide an insight that could lead the design of new syntheses.

2 Computational details

To systematically identify all the $sp-sp^2$ carbon systems in the GDY family, we used ToposPro to generate subnets of graphene where bonds are deleted in all possible ways and substituted by linear diacetylenic units (see [52] for details). Based on the 2D crystal structures selected by ToposPro, periodic boundary condition (PBC) DFT simulations have been carried out by employing CRYSTAL17 to optimize the geometry (both the atomic position and cell parameters) and to compute the Raman and IR spectra. We adopted the hybrid exchange–correlation functional PBE0 together with the 6-31G(d) Gaussian basis set. This level of theory has been chosen according to our previous investigations of the structural and vibrational properties of γ -GDY and related nanoribbons, in which we compared the results obtained using different

functionals and basis sets [31]. When using the 6-31G(d) basis set in PBC-DFT simulations with the CRYSTAL code, the exponent of the diffuse sp orbitals of carbon atoms has been increased from 0.1687144 to 0.187 Bohr⁻² to avoid convergence problems in the SCF [53], due to basis set linear dependencies. Considering the other simulation parameters, the tolerance on integral screening has been fixed to 9,9,9,9,80 (TOLINTEG parameters), whereas the shrink parameters defining Monkhorst–Pack and Gilat sampling points have been fixed to 50 for the prediction of the vibrational properties. We report unscaled wave-number values both in the discussion and in the figures (a suitable scaling factor should be defined whenever comparing these theoretical spectra with experimental ones, see [54]). To ease the comparison among the different crystals, we adopted the same Cartesian reference system with the z -axis orthogonal to the 2D crystal plane. When useful, a local reference system (x' , y' , z') is introduced for the description of physical quantities characteristic of the linear diacetylene branches: the x' axis is oriented along the sp chain and z' parallel to the z -axis of the crystal.

3 Results and Discussion

In our previous paper [52], we developed an approach to generate and classify all possible GDY/GZY 2D structures. We considered stable graphene derivatives by inserting linear diacetylene (C4) groups in the primitive cell. Our approach is based on removing edges from the graphene structure and substituting them with linear diacetylenic units. With the help of the topological classification tools in ToposPro, we extracted 332 topologically distinct patterns and then, by defining five building blocks, here named h (small hexagon), H (large hexagon), R (rhombus), T (triangle), L (line), we extracted only those containing possible building blocks that allow to tile the plane without a large distortion. By such procedure we obtained 26 GDY-like structures, of which 17 are new. The structures are named as $6-h^mL^nT^pR^q$, where 6 represents the number of carbon atoms along the longest edge and the superscript on the building block symbols represents the number of each block appearing in the primitive unit cell.

3.1 Electronic features and molecular structure

We focus first on 6-L, 6-H (also known as α -GDY [15, 16]), and 6-R, which are characterized by the simplest topologies of a single repeating unit (line, large hexagon (H) and rhombus (R), and on 6-hT² and 6-HT² which are the two widely studied polymorphs of graphdiyne also called γ -GDY and β -GDY (respectively) [15, 16]. A second family of 2D crystals (hereafter referred as grazdynes, GZY) contains linear diacetylene chains (L) and extended sp^2 domains forming zig-zag sequences of CC bonds like polyacetylene and/or ribbons made by condensed aromatic rings with L chains linked to the zig-zag edges. All these systems are sketched in Figure 1.

The electronic structures of the 2D crystals under investigation display some common characteristics. A simplified description of the crystal orbitals, following the theory of molecular orbitals as linear combination of atomic orbitals (MO=LCAO) and applied to the minimal set consisting of the hybrid atomic

orbitals (AO) belonging to the valence shell of the carbon atom, gives us some useful insights. In particular, it allows highlighting the possible role and interactions of sp^2 -C vs sp -C in determining the molecular architecture (e.g., bond lengths) as well as physical properties (e.g., the spectroscopic response). The orbitals belonging to the highest energy occupied bands and to the lowest energy unoccupied bands should mainly arise by the combination of p_z orbitals of sp and sp^2 hybridized carbon atoms and by the combination of the p_y orbitals of the sp -carbon chains. Moreover, because of the mirror symmetry to the crystal plane, π_z orbitals coming by the mixing of p_z cannot mix with σ orbitals from any combinations of p_y orbitals.

We underline that: (i) The different crystal structures and the topology of the bond network rule the features of the π_z orbital, which could involve the whole set of p_z AOs (with similar weights of the p_z AO from sp^2 - and sp -carbon atoms) or could be preferentially localized either on sp^2 - or on sp -carbon atoms. According to the above property of π_z orbitals, the resulting electron charge density is fully delocalized over the whole crystal network or is mainly localized either on the individual diacetylene segments or on sp^2 domains. (ii) Since the p_y AOs of sp carbons possess even mirror symmetry with respect to the xy plane, they can mix with the sp^2 -hybridized AOs of the sp^2 -carbon atoms (same even symmetry), and therefore may participate to the σ orbitals system. However, based on energy considerations and local symmetry (they are odd with respect to the vertical mirror plane $x'z'$ whereas the sp^2 hybrids are even), this mix is negligible and p_y AO should concur to the formation of well-localized MO on the individual diacetylene segments. Electrons sitting in these orbitals impart the quasi-triple bond character exhibited by the two bonds adjacent to the central diacetylene quasi single CC bond (P_i label in Fig. 2). (iii) Considering point i) each of the crystals presented in Fig. 1 possesses an extended network of p_z electrons (one p_z AO at every C site), which possibly give rise to highly delocalized electron density. On the other hand, the delocalization properties are modulated by the interplay between the sp and the sp^2 phase, which depends on the selected crystal structure. This feature strongly affects the degree of π -conjugation among different diacetylene chains.

Since the vibrational spectrum (notably Raman) of sp carbon chains is very sensitive to the delocalization properties of the π electrons, as well as to end group effects [33], we analyse the computed spectra of GDYs and GZYs, focusing mainly on the vibrational transitions involving the diacetylene branches.

Table 1. For each structure the energy contribution per carbon atom, referred to graphene (ΔE) and bond alternation parameter (BLA) of the polyynes units are reported in the table, together with the number and symmetry species of polyyne ECC phonons.

structure	ΔE (kcal mol ⁻¹)	BLA (Å)	ECC modes
6-H (α -GDY)	27.39	0.142	$1A_g + 1E_{2g}$
6-L	26.18	0.136	$1A_g$
6-R	25.48	0.154	$1A_g + 1B_{1g}$
6-HT ² (β -GDY)	25.40	0.156	$1A_g + 2E_{2g}$
6-hT ² (γ -GDY)	21.13	0.167	$1A_g + 1E_{2g}$
6-hL	20.59	0.138	$1A_g$
6-hL ²	23.11	0.136	$2A_g$
6-hL ³	24.06	0.135	$3A_g$
6-h ² L	16.81	0.139	$1A_g$

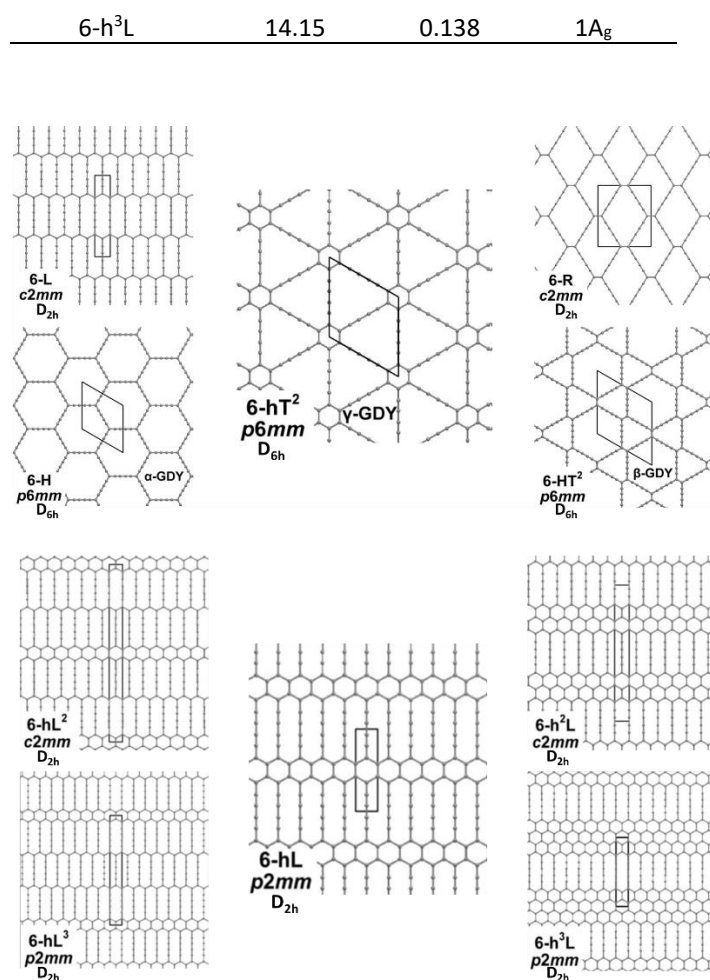


Figure 1: Sketch of the 2D-GDY (top) and 2D-GZY (bottom) structures analysed. For each structure the unit cell, plane group and point group symmetry (factor group at Γ point of BZ) are illustrated.

3.2 Vibrational spectra of GDY

We start by defining the internal and symmetry CC stretching coordinates of the diacetylene branches. This allows establishing the peculiar group vibrations of the chains that are involved in the Raman and IR active $q=0$ phonons, with no need of calculation. For each diacetylene branch (labeled by the i index) we consider the sequence of the five CC bonds forming the 6 carbon atoms chain, and we define the relative stretching coordinates ($r_i, r'_i, T_i, T'_i, P_i$) as indicated in Figure 2. We also define the group coordinates $\{S_i\}$ sketched in Figure 2: the symmetric (T_i^+) and the antisymmetric (T_i^-) combination of quasi-triple CC bonds stretching; the symmetric (r_i^+) and the antisymmetric (r_i^-) combination of the terminal quasi-single CC bonds stretching, and the stretching of the central quasi-single CC bond (P_i). The group coordinates defined above are symmetry coordinates for the diacetylene fragment, showing an inversion centre in the middle of the central CC bond.

In most crystal structures illustrated in Fig. 1 and Table S1 in SI, the inversion centres carried by each diacetylene unit are preserved, so the collection of the sets $\{S_i\}$ define a symmetry adapted internal coordinates basis set, useful for the interpretation of the spectral features of the crystals. This happens for the crystals 6-H, 6-L, 6-R and 6-hT², whereas in 6-HT² the inversion centres located on the chains are lost.

Remarkably, for all the crystals but 6-HT², we can state that within the $\{S_i\}$ set only the subset of gerade coordinates $\{S_k\}^g = \{r_i^+, T_i^+, P_i\}$ is involved in the Raman active phonons, while the subset of ungerade coordinates $\{S_k\}^u = \{r_i^-, T_i^-, P_i\}$ is involved in the IR active phonons. This feature is independent on the number of diacetylene chains in the unit cell and on the kind of the chemical group linking the chains. On other hand, the symmetry of the crystal and the number of chains will determine the suitable symmetry combinations of the $\{S_k\}^g$ of the different chains, giving Raman active phonons. The A_{1g} and E_{2g} linear combinations of the $\{S_k\}^g$ coordinates of different chains describe the Raman active phonons of the crystals possessing D_{6h} symmetry (6-H, and 6-HT²). In the 6-L and 6-R structures (D_{2h} symmetry) such linear combinations give rise to B_{1g} and A_g Raman active phonons. Similarly, linear combinations of $\{S_k\}^u$ coordinates give E_{1u} IR-active phonons in D_{6h} structures and B_{3u}/B_{2u} IR-active phonons in D_{2h} structures.

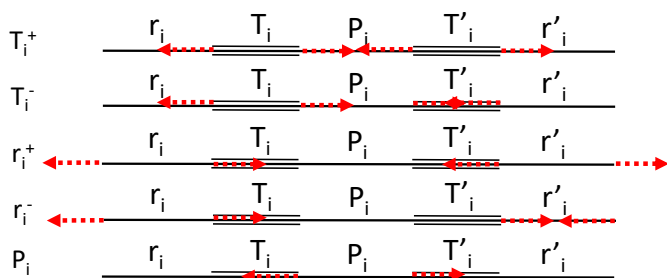


Figure 2. Definition of the CC stretching internal coordinates and sketches of their symmetry adapted combinations $\{S_k\}$.

Vibrational displacements located in the sp^2 domains will also concur to the definition of the vibrational trajectories associated to the phonons, giving rise to rather complex patterns of collective atomic displacements. Luckily, the definition of the sets $\{S_k\}^g$ and $\{S_k\}^u$ greatly eases the analysis of the spectral features of the more informative spectral region – above 2000 cm^{-1} , mainly involving vibrations of the diacetylene branches.

In Figure 3 we report the computed Raman and IR spectra for the investigated GDY series. Frequencies of the optical phonons and predicted Raman and IR band intensities are shown in Table S2, together with the classification of the phonons according to the suitable point group symmetry (namely the factor point symmetry group at the Γ point of the first Brillouin Zone BZ). In Table 2 we decided to report only those phonons with high vibrational frequency ($> 2000\text{ cm}^{-1}$) that are related to stretching modes of the diacetylenic chains.

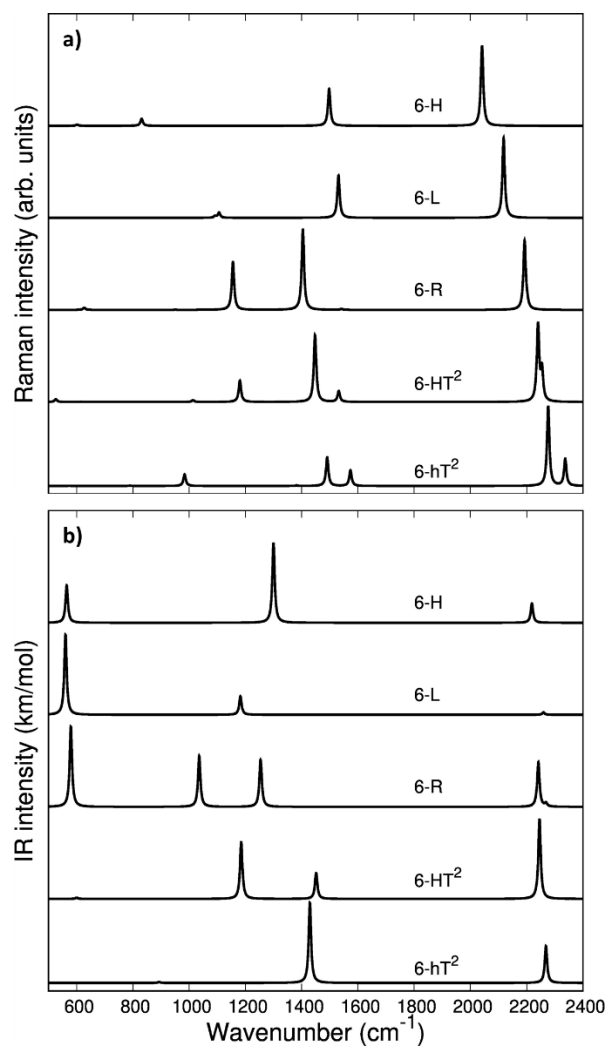


Figure 3. Computed Raman (a) and IR (b) spectra of GDY systems: 6-hT², 6-HT², 6-R, 6-L and 6-H.

The vibrational spectra of GDYs, show two characteristic regions. The $2000\text{--}2400\text{ cm}^{-1}$ interval is typical of the stretching modes of the CC triple bonds. The vibrations of the sp -carbon chains give rise to strong Raman active bands above 2000 cm^{-1} , which can be considered the marker bands of the diacetylenic units. In the lower frequency region ($800\text{--}1600\text{ cm}^{-1}$), we find Raman active bands assigned to the stretching vibrations of the CC bonds linking sp^2 hybridized carbon atoms, *i.e.*, bonds belonging to aromatic rings (case 6-hT²) or the CC bonds linking the diacetylene branches in 6-L, 6-R, 6-HT². Such phonons always involve additional contributions from the stretching of the quasi-single bonds belonging to the sp -carbon chains.

ARTICLE

Table 2. Computed wavenumbers (spectral region above 1800 cm^{-1}), symmetry species, relative Raman activities and IR band intensities for the $q=0$ Raman or IR active phonons of the GDY and GZY crystals. Relative Raman activities are calculated by assigning the value of 1000 to the strongest Raman transition of the whole spectrum.

2D- GDY structures					
Crystal	Raman Spectrum			IR spectrum	
	wavenumber (cm^{-1}) (Irrep)	Raman activity	Vibrational assignment	wavenumber (cm^{-1}) (Irrep)	IR intensity (km mol^{-1})
6-H	2041 (E_{2g})	1000	ECC	2219 (E_{1u})	365
	2361 (A_{1g})	0.02	ECC		
6-L	2118 (A_g)	1000	ECC	2260 (B_{3u})	2
6-R	2193 (A_g)	1000	ECC	2241 (B_{3u})	267
	2202 (B_{1g})	57	ECC	2269 (B_{2u})	20
6-HT²	2240 (E_{2g})	142	partial ECC character	2246 (E_{1u})	1501
	2240 (A_{1g})	1000	ECC	2356 (E_{1u})	2
	2255 (E_{2g})	453	partial ECC character		
6-hT²	2277 (A_{1g})	1000	ECC	2269 (E_{1u})	480
	2337 (E_{2g})	344	ECC		
2D-GZY structures					
Crystal	Raman Spectrum			IR spectrum	
	Wavenumber (cm^{-1}) (Irrep)	Raman activity	Vibrational assignment	Wavenumber (cm^{-1}) (Irrep)	IR intensity (km mol^{-1})
6-hL	2248 (A_g)	328	ECC	2255 (B_{3u})	8719
6-hL²	2205 (A_g)	1000	partial ECC character	2255 (B_{3u})	584
	2244 (A_g)	358	partial ECC character	2310 (B_{3u})	58
6-hL³	2173 (A_g)	1000	ECC	2219 (B_{3u})	444
	2245 (A_g)	107	$C\equiv C$ str	2256 (B_{3u})	248804
	2313 (A_g)	15	ECC	2292 (B_{3u})	88
6-h²L	2257 (A_g)	1000	ECC	2250 (B_{3u})	640
6-h³L	2224 (A_g)	387	ECC	2247 (B_{3u})	512

ARTICLE

Vibrational transitions in the 2000 -2400 cm^{-1} range. The higher frequency region of the Raman spectrum of GDYs shows the strongest transitions of the whole Raman spectrum. According to our symmetry analysis, for D_{6h} structures (6-H and 6-hT²) we can predict two Raman active phonons resulting from the A_{1g} and E_{2g} (doubly degenerate) combination of the symmetric triple bond stretching (T_i^+) of the three diacetylene chains belonging to the hexagonal cell. For 6-R and L crystals, we have two (A_g and B_{1g}) transitions and one only A_g transition, respectively, according to the number of chains in the primitive cell - two and one chain, respectively.

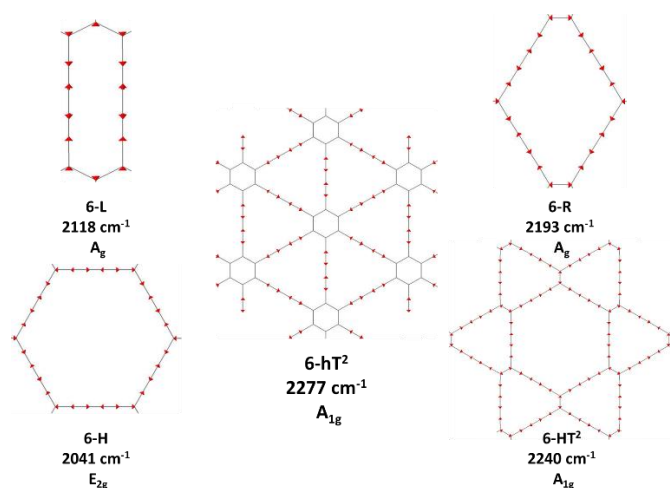


Figure 4. Sketches of the vibrational eigenvectors associated to the strongest Raman active ECC phonons of GDYs. The corresponding vibrational wavenumbers and symmetry species are reported.

A peculiar case is that of 6-HT² crystal, with a cell containing six diacetylene branches, which lost their local inversion centre in the crystal. In this case, we obtain one A_{1g} and two E_{2g} bands, with the E_{2g} transition at 2240 cm^{-1} and the A_{1g} transitions showing accidental degeneracy. In 6-HT² the two E_{2g} phonons mix T_i^+ and T_j^- group coordinates of different chains, while the A_{1g} phonon corresponds to the in-phase combination of the six T_i^+ , similar to the other GDYs (see Figure 4 and SI). With the only exception of the E_{2g} vibrations of 6-HT², the Raman active phonons in the 2000-2400 cm^{-1} region show, for all the diacetylene branches, the characteristic pattern of the Effective Conjugation Coordinate (ECC) mode. In our case, the ECC is a collective simultaneous $\text{C}\equiv\text{C}$ stretching/ $\text{C}-\text{C}$ shrinking of the bonds forming the diyne segments (see sketches of the vibrational eigenvectors in Figure 4 and SI). Indeed, the group coordinates T_i^+ are dynamically coupled with the other stretching degrees of freedom of the sp chain, thus giving rise to collective vibrations, involving also stretching vibrations of the quasi single CC bonds, namely of the sub-sets of coordinates $\{r_i^+, P_i\}$, which oscillate out-of-phase with T_i^+ , during the ECC vibration. The remarkable dynamic coupling between triple and

single bonds stretching in sp chain, resulting in ECC-modes, is a well-recognized phenomenon, encountered for a wide variety of oligoynes, irrespective of their chain length and end groups [33, 55-58]. The high Raman activity of the ECC modes and the sensitivity of their frequency to π -electron conjugation have been widely investigated in the past and are reported as the signature of the strong electron-phonon interaction that takes place along the ECC vibrational trajectory [55, 57-58]. The ECC vibration can be described as the oscillation of the bond length alternation (BLA) parameter, which is the key vibrational parameter affecting the electronic structure of carbon chains with polyconjugated π electrons [55, 57-58].

Interestingly, in GDY crystals, the occurrence of a shrinking of the C-C bonds of the sp chain that is simultaneous with the $\text{C}\equiv\text{C}$ stretching not only depends on the dynamical coupling, but is a direct consequence of the translational symmetry of the crystal. It requires that $q=0$ phonons are such that the atomic displacements do not modify the cell volume, at any time. Indeed, during ECC vibrations, the shrinking of the C-C bonds (implied by contributions from P_i and r_i^+) does guarantee the fulfilment of such translational symmetry constraint when the two $\text{C}\equiv\text{C}$ bonds of diacetylene segment stretch in phase (T_i^+).

Looking at Figure 3, we observe for the 6-hT² system two distinct bands at rather different frequencies associated respectively to the A_{1g} symmetry ECC phonon (2277 cm^{-1}) and to the E_{2g} ECC phonon (weaker band at 2337 cm^{-1}). In a previous paper [31] we showed that the sizeable difference in wavenumber of these two phonons (60 cm^{-1}) is due to the interaction among adjacent diacetylene chains, linked through the CC bond belonging to the phenyl unit. The separation in frequency between such ECC modes is smaller in other GDYs, while in the most cases the intensity of the totally symmetric A_{1g} (or A_g) line is the largest one. However, 6-H represents a peculiar exception in the GDY family: in this case, the ECC E_{2g} phonon has the largest Raman activity, while the A_{1g} phonon is practically silent (it is 10^{-5} times weaker than the E_{2g} ECC phonon -see Table 2 and S2). Interestingly, for 6-H the frequency of the E_{2g} phonon is very low (2041 cm^{-1}), and remarkably lower than that of the A_{1g} mode, (2361 cm^{-1}) which is up-shifted by 320 cm^{-1} . Such features indicate that, at difference from the other GDYs, the effect of the interactions between diacetylene chains through one only sp^2 carbon atom cannot be described anymore as a weak perturbation of the physics of the individual sp chains. In other words, the vibrational dynamics and the Raman response of 6-H is heavily affected by the extended network of conjugated π^z -electrons involving all the diacetylene branches, linked by the one sp^2 carbon atoms supporting the threefold branching.

As result of the different behaviours commented above, the higher frequency region of the GDY series shows a very simple Raman pattern, with a strong ECC line, which is accompanied in 6-hT² and 6-HT² by only one clearly observable weaker satellite band, located at higher frequency (see Figure 3).

Figure 3 shows that the main ECC line follows a decreasing frequency trend as a function of the crystal structure, spanning a wide interval of about 300 cm^{-1} , along the sequence: 6-hT², 6-HT², 6-R, 6-L and 6-H (from the higher to the lower ν_{ECC}). This decreasing trend of ν_{ECC} parallels the increasing π -conjugation of the diacetylene chains, as observed elsewhere [31-33, 55, 57-58]. This frequency behaviour is commonly reported in polyconjugated sp chain molecules [33, 55, 57-58] in conjunction with the equalization of the equilibrium bond lengths (i.e. small BLA values). A similar behavior of decreasing BLA values with increasing π -conjugation is observed also in the present case (see Table 1 and Table S1).

In [52], a comparative study of the energy of several GDY crystal is reported. The crystal energy, normalized to the number of C atoms, is referred to the case of graphene, showing that the introduction of diacetylene units has an energy cost (positive ΔE , see values in Table 1 and S1). Moreover, ΔE values for the GDY series show a marked dependence on the crystal structure, e. g. on the relative abundance of sp² and sp phase and bonds topology: the most stable system is 6-hT², while the higher energy system is 6-H.

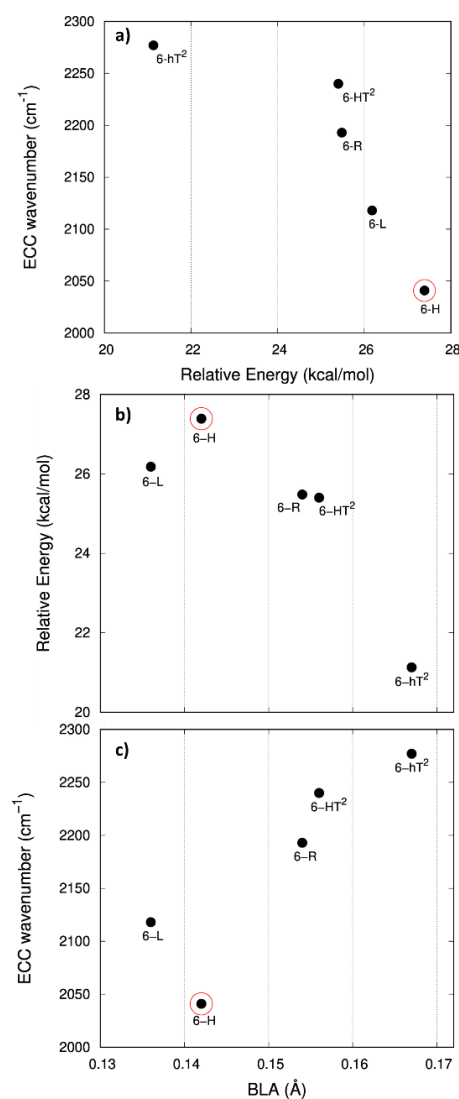


Figure 5. Correlation between physical quantities sensitive to π -electrons conjugation. Panel a: ECC phonon wavenumber vs. ΔE (ΔE is the relative crystal energy -

per atom -referred to graphene, see text). Panel b: ΔE vs. BLA parameter. Panel c: ECC phonon wavenumber vs BLA. The data corresponding to 6-H crystal are highlighted by a red circle.

In Figure 5.a we report the plot of ν_{ECC} vs ΔE , which show a nice correlation: ν_{ECC} softens as ΔE increases. Considering the high reactivity of the sp carbon chains characterized by a cumulene-like structure (i. e. an sp chain ideally approaching a linear sequence of double bonds), we expect that the systems showing higher ΔE values also present a chain structure with more equalized CC bonds. The BLA parameter, which measures the average degree of bond alternation in the sp chains, provides an estimate of this property. The BLA parameter has been obtained as the difference between the average bond length of quasi single bonds and the average bond length of the triple ones:

$$\text{BLA} = 1/3 (r_0+r_0'+P_0) - 1/2 (T_0+T_0')$$

where r_0 , P_0 and T_0 are the equilibrium bond length values of the CC bonds belonging to the diacetylene chains (see Figure 2 for the meaning of the symbols).

The BLA values of GDYs, reported in Table 1, are compared to ΔE in the plot in Figure 5.b, showing the expected correlation. This plot nicely explains the observed correlation between energy and ECC frequency: as a matter of fact, the usual trend among ν_{ECC} and BLA values is indeed verified (Figure 5.c).

A closer look at Figure 5, shows that there is a frequency value, namely that of the 6-H crystal, which does not follow the approximately linear trend of ν_{ECC} with BLA. Indeed, 6-H shows an ECC frequency remarkably low in comparison with its BLA. Moreover, also in the plot of ΔE vs. BLA (Figure 5.b), the 6-H crystal is not within the trend. It seems that the predicted chain geometry does not fully reflect the very high electron delocalization described by ν_{ECC} and ΔE . Notice moreover that the 6-H structure also shows a peculiar vibrational feature, namely a dominant ECC band of E_{2g} symmetry, which would deserve further investigations.

We tried to rationalize the origin of the different degree of electrons conjugation in GDYs, by considering the different characteristic of the sp² linkers. As reported in [31], the high aromatic character of the phenyl units prevents an effective conjugation of the π_z -system of the ring with the π_z -electrons of the grafted diacetylenic segments, which results in the large BLA and rather high frequency of the ECC Raman band of 6-hT². Instead, the sp chains belonging to 6-HT² and 6-R, are linked to each other through just one CC bond formed between two sp² C atoms (i.e., through a formal double bond). This kind of linker is more prone to share its π_z electrons with the π_z -electron system of the diacetylene units. Thus, 6-HT² and 6-R show intermediate ECC frequency and BLA values. Also in 6-L, which features arrays of sp² C atoms forming zig-zag chains with equalized CC bond length – a polyacetylene-like chain - one can identify pathways consisting of an infinite sequence of sp chains bridged by one CC bond formed by sp² C atoms. In this case the p_z electrons of the sp² C atoms belongs to a fully delocalized π system along the zig-zag chain which is more effective in promoting π^2 -electron conjugation with the sp branches. The 6-L structure is at the second place if one considers the trend of ΔE and of ECC frequency (from lower to higher frequency values). A furtherly enhanced tendency toward π -conjugation is observed in 6-H, with just one sp² C atom acting as node of

the network of diacetylene chain, showing the lower ECC frequency, in correspondence with the higher instability of the crystal (higher ΔE).

For most GDYs ν_{ECC} shifts toward lower values as the ratio between the number of sp and sp² C atoms (sp/sp²) decreases. As observed in [52], the sp/sp² ratio also correlates with the relative energy, showing a general increase with the increase of the sp phase content. 6-L is the only exception to this trend and it possesses a very low ν_{ECC} and a high ΔE value but, in contrast, it features a low sp/sp² carbon ratio: this observation tell us that also the topology of the sp² phase can play a very important role.

The infrared spectra of the higher frequency region is characterized by phonons involving the antisymmetric stretchings of the triple bonds (T_i^-) accompanied by out of phase contributions of (r_i^-). Because of the inversion symmetry, IR active phonons cannot involve the stretching of the central CC bonds.

In the D_{6h} systems featuring three sp branches in the cell (6-H, 6-hT²) we find only one IR active (doubly degenerate) E_{1u} phonon and we find one more E_{1u} phonon in the case of 6-HT² (with six sp branches). 6-L shows just one B_{3u} transition and 6-R two (B_{3u} and B_{2u}) transitions, according to the number of branches belonging to the primitive cell. Looking at the IR intensity values (Table 2), it is immediate to realize that, also in presence of two IR active modes, only one band is strong enough to be identified in the plot of the simulated IR spectra. In the framework of ECC theory [33, 55], such IR active modes have been described as the BLA oscillation with a node in the middle of the chain. Differently from the collective ECC modes, the vibrational frequency of these modes is not much sensitive to the degree of conjugation of the chain, especially in the case of short sp chains, moreover their frequency is always higher than ν_{ECC} . The above characteristics reflect also in the spectral trend, showing a modest dependence of the position of the high frequency IR bands on the different crystal structures of the GDY series.

Vibrational transitions below 1600 cm⁻¹. The Raman transitions in this region correspond to phonons involving the stretching of the “quasi” single bonds of the sp chains. For a given i-th sp chain, the r_i^+ and P_i coordinates are involved in out-of-phase combination ($r_i^+-P_i$), which fulfils the requirement that the cell volume is preserved during the vibrational displacements. The stronger Raman line in this region has a frequency value in the range 1550 – 1480 cm⁻¹ (see Tables S2 and S3) and belongs to the totally symmetric species for all the crystals. However, for 6-H, which shows a strong E_{2g} ECC transition, also the $r_i^+-P_i$ phonon belongs to E_{2g}.

Table 3. Bond length of the quasi single CC bonds belonging to the diacetylene branches, for GDY structures. For meaning of bond labels, see Figure 2.

GDY	6-R	6-HT ²	6-hT ²	6-H	6-L
P (Å)	1.343	1.345	1.351	1.336	1.329
r (Å)	1.398	1.399	1.406	1.391	1.381
ν (C-C) (cm ⁻¹)	1404	1448	1491	1498	1531

Table 3 shows that there is a nice correlation between the strength of the quasi-single CC bonds belonging to the sp chain

and the frequencies of the associated CC stretching phonons for the series 6-R, 6-H, 6-R: the shorter the bonds, the higher is the frequency. 6-HT² and 6-hT² do not follow this trend, likely because of the coupling with ring breathing vibration in 6-hT² and because of the more complex vibrational structure of 6-HT², the crystal with the largest unit cell. However, the vibrational eigenvectors become much more complex in presence of bonds linking sp² carbon atoms, which are possibly subjected to strong dynamical coupling with r_i stretchings. Also vibrational modes rather localized in the sp² domain can occur, as in the case of 6-hT², for which the nature of these vibrations has been discussed in our previous paper [31]. In particular, the three bands located at 1382, 1491 and 1574 cm⁻¹ show large contributions by stretching vibrations of the phenyl units, as reported in Table S3 of the SI.

The collective character of the phonons of GDYs in the lower frequency region (below 1400 cm⁻¹) makes difficult to propose a comparative discussion. We limit ourselves to the observation that 6-R and 6-HT², which both feature isolated sp² CC bonds between diacetylene chain, present a strong band close to 1100 cm⁻¹ which is characterized by a vibrational eigenvector showing a remarkable contribution from the linker sp² CC bond (see Table S3). Turning to the analysis of the IR spectra in the region below 1600 cm⁻¹, we focus our attention on the possibility to identify different marker bands for the different 2-D structures. For 6-H one can find a very intense IR band at 1300 cm⁻¹. Also for 6-hT², the peak with the highest IR intensity is located below 1500 cm⁻¹: we compute a strong band at 1429 cm⁻¹ with contributions from stretching vibrations of the bonds of the phenyl units (see Table S3). The marked frequency difference between such IR bands of 6-H and 6-hT² ($\Delta\nu = 129$ cm⁻¹) gives the possibility to distinguish between the two structures.

The IR spectra of both 6-HT² and 6-R show two strong IR-active bands, well separated in frequency and located at different positions for the two systems. Looking at the vibrational eigenvectors, we can describe these vibrations as mainly characterized by the in phase T_i^- and r_i^- . Also for these systems, IR spectroscopy shows strong distinctive features, useful for their identification.

6-L shows an isolated band located at 1182 cm⁻¹ very close to the one of 6-HT² (1185 cm⁻¹). However, for 6-HT², the presence of the additional strong band of 6-HT² at 1452 cm⁻¹, allows distinguishing among the two crystals. Moreover, the whole intensity pattern is different for the two structures.

In the lower frequency region (< 600 cm⁻¹, see Figure 3) it is possible to identify different marker bands. Indeed, a very intense IR active peak appears for 6-R, 6-L and 6-H, located respectively at 580 cm⁻¹, 560 cm⁻¹ and 565 cm⁻¹. Through the analysis of the vibrational eigenvectors associated to these bands (SI) these phonons are characterized by collective in-plane bending of the CC bonds of the sp chains.

3.3 Vibrational spectra of GZY

The second class of crystals studied in this work consists in the series also known in literature as grazynes [59]. They are 2D materials made by condensed aromatic rings forming ribbons

with different widths connected by L units (diacetylene chains) (Figure 1) [59]. For the analysis of the Raman and IR spectra of GZY we will focus our attention on the evolution of the spectra inside two different families, whose structures are depicted in Figure 1.

The first one (GZY-I) (6-hL , 6-hL^2 , 6-hL^3) shows a topology made by ribbons consisting in an infinite sequence of condensed h units (only one h unit in the height, forming a polyacene chain), intercalated by layers formed by L units. These layers have different height, depending on the number n of L units ($n = 1, 2, 3$), running parallel to the layer width (x axis direction) and linked each other through zig-zag polyacetylene-like sp^2 chains. The 6-L crystal, already discussed as a member of the GDY group, is a limiting case of the GZY-I family and will be considered in our comparative analysis.

The second family (GZY-II) is characterized by a layer of parallel L segments (the layer thickness corresponds to only one L unit) intercalated to nanoribbons formed by condensed h units, with different widths, according to the notation: 6-hL , $6\text{-h}^2\text{L}$, $6\text{-h}^3\text{L}$. Graphene can be considered a limiting case, belonging to this family. In Figure 6 we report the Raman spectra and the infrared spectra calculated for the GZY-I and GZY-II groups.

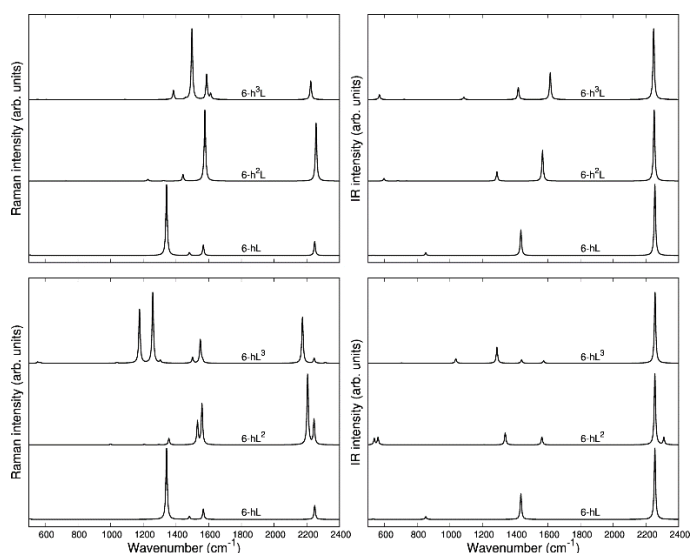


Figure 6. Calculated Raman spectra (left) and IR (right) spectra of GZY-I (top) and GZY-II (bottom).

The Raman spectra of GZYS show features typical of the sp phase, which is the main responsible of the characteristic vibrational features in the high frequency (above 2000 cm^{-1}) and of the graphene-like ribbons, which give rise to features below 1600 cm^{-1} . The interplay between the sp and sp^2 phases influences the degree of π electrons delocalization in the whole crystal and is expected to have a signature especially in the Raman spectra, which cannot be regarded by a mere superposition of the spectroscopic response of the L layers and of the h ribbons. Because of the complex trajectories of the phonons below 1600 cm^{-1} , involving atomic displacements in both sp and sp^2 phase, the following discussion will be focused on the vibrational features coming from vibrations mainly

localized on the diacetylene branches, which are found in the $2000 - 2400\text{ cm}^{-1}$ region.

Raman spectra. The $q = 0$ phonons of GZY-I are classified according to the D_{2h} symmetry: Raman transitions in the high frequency range are associated to A_g phonons. Table 2 lists frequencies and intensities of these lines, which are as many as the number of sp chains belonging to the primitive cell. As in the case of GDY, one strong Raman line, possibly accompanied by satellite lines located in the higher frequency side, dominates the sp spectral region (Figure 6).

The eigenvectors analysis (Table 4) shows that only chains which carry a symmetry inversion centre develop a collective ECC vibration, namely the symmetric stretching of quasi triple bonds (T_i^+) accompanied by out-of-phase vibration of the quasi single bonds (r_i^+ , R_i). This happens for 6-hL , and for the central chains of the L layer of 6-hL^3 . Chains that have lost the inversion symmetry give rise to phonons characterized by displacements localized either on the triple bond close to the zig-zag chain, or close to the polyacene ribbon. This is the case of 6-hL^2 : its strongest Raman active transition corresponds to a phonon describing a BLA oscillation along a path crossing a CC bond belonging to the zig-zag chain, and does not involve the peripheral $\text{C}\equiv\text{C}$ bond of the L^2 layer. Its low frequency and high intensity should be ascribed to delocalization of the π_z electrons phenomena, which are coupled to the CC bonds of the polyacetylene-like chain. In a similar way, we can justify the large Raman intensity (and low frequency) of the ECC-like mode of 6-hL^3 . It can be described as due to the ECC vibration of the central chain (showing inversion centre) accompanied by the in phase BLA oscillation of the two adjacent chains, localized on the $\text{C-C}\equiv\text{C}$ sequence close to the zig-zig chain.

In the GZY-II family the situation is simpler because all these structures contain only one L segment in the primitive unit cell, which is characterized by inversion centre. Thus, this family shows only one A_g transition above 2000 cm^{-1} , corresponding to the ECC mode of the diacetylene chain. This implies only one Raman line in the higher frequency region of the Raman spectrum.

Interestingly, by looking at the calculated Raman spectra we can see that the GZY-II series shows a little dispersion of the ECC line, whereas for the GZY-I series the ECC – like phonon shows a dispersion of 130 cm^{-1} , with a decreasing frequency trend as the number of L segments in the L layer increases. This is another evidence that the CC bonds belonging to the zig-zag chain bridge the chains in such a way that sizeable electrons conjugation between the diacetylene segments occurs.

As observed in 6-hT^2 , aromatic systems are less prone to share π -electrons with the sp system, and this explains why the frequencies of the ECC bands of the GZY-II series are rather high and little sensitive to the width of the graphene-like ribbons.

As a last observation, we notice that the modulation of the ECC phonon frequency is remarkably stronger in GDY (dispersion of about 300 cm^{-1}) than in the whole GZY family (dispersion of 140 cm^{-1}).

In Figure 7.a we illustrate the correlation between the frequency of the ECC line and the crystal relative energy ΔE defined above. Similar to the case of the GDY family, we find a

decreasing trend of the ECC frequency as the crystal become less stable. Also in this case larger ΔE values correspond to less stable sp chains, showing a more cumulene like character (more equalized CC bonds). Figure 7.a and Figure 7.c shows the expected trend of the ECC frequency versus ΔE and BLA.

Interestingly, also for the GDZ family there is an outlier, namely 6-h³L, showing its ECC frequency (2224 cm⁻¹) rather low in comparison with its ΔE . Moreover, also its BLA value does not correlates well with the energy value.

Table 4. Sketches of the vibrational eigenvectors associated to the Raman active (A_g) phonons of GZY-I group, in the spectral region above 2000 cm⁻¹. In the last row the corresponding vibrational wavenumbers are reported.

6-hL	6-hL ²	6-hL ³	6-L
2248 cm⁻¹	2205 cm⁻¹	2244 cm⁻¹	2173 cm⁻¹
		2245 cm⁻¹	2313 cm⁻¹
			2118 cm⁻¹

A possible rationalization of such behaviour should consider the role of the sp^2 phase, that also contribute to ΔE : notice that for 6-h³L the sp/sp^2 ratio is the lowest in the series (0.5).

IR spectra. Above 2000 cm⁻¹ the GZY crystals show IR active B_{3u} transitions characterized by dipole moment oscillations along the direction of the sp chains (x axis). Similar to their Raman counterpart, the number of IR active transitions equals the number of L units in the primitive cell. However, the IR spectrum shows only one band in most cases because of the very low IR intensity of the other transitions. Only in 6-hL² a satellite band can be observed in the IR spectrum, at higher frequency with respect to the main line (Figure 6).

The stronger IR line in this region corresponds, for all the GZY crystals, to the out of phase stretching (T_i^-) of the triple CC bonds of the chain. In cases with more than one chain per unit cell, it is described by the in-phase combination of T_i^- of all the chains (see the vibrational eigenvectors sketched in Table 5). Interestingly, by looking at the data reported in Table 2, we can realize that phonons corresponding to similar displacements of the sp carbon can have very different IR intensities in the different crystals. In particular, 6-hL³ shows a remarkably high IR intensity of the band at 2256 cm⁻¹ which could be ascribed to relevant charge fluxes associated to the collective vibration of

the three L segments forming the L³ layer. This last observation can be taken as further evidence of the high delocalization of π electrons along the sequence made by three diacetylene segments.

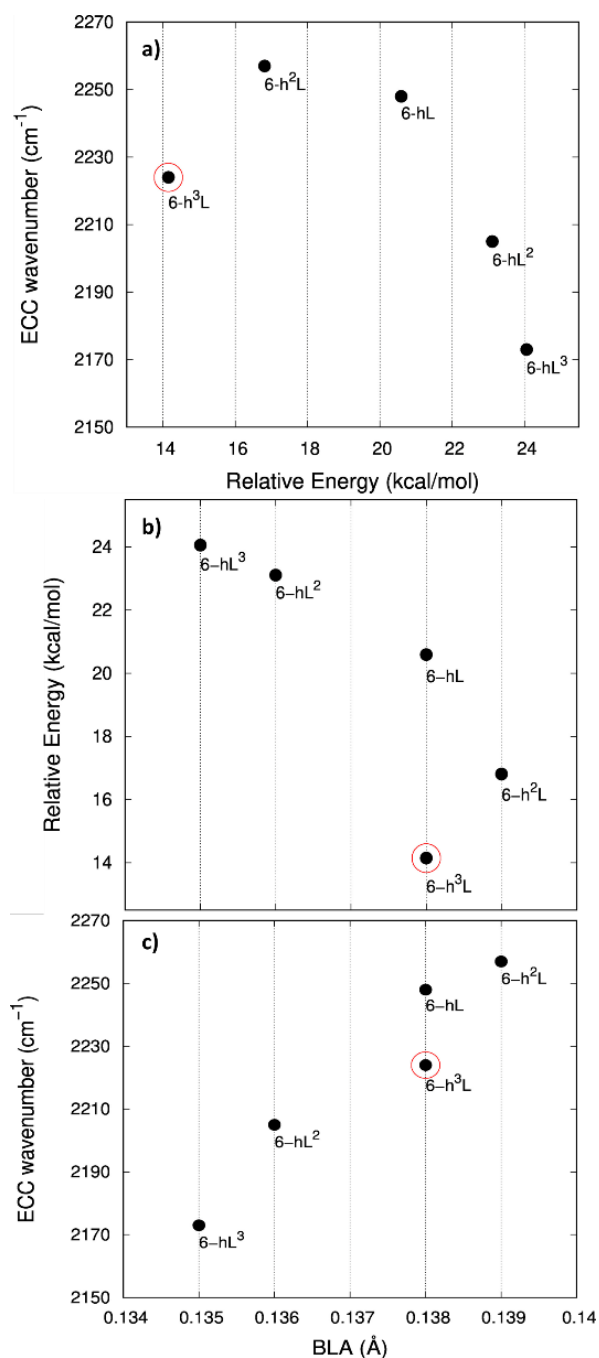
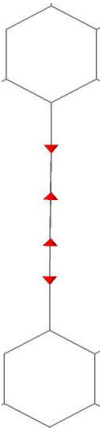
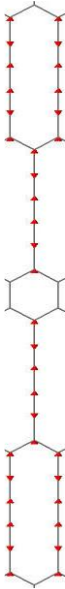

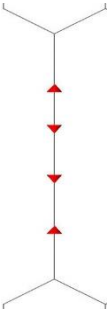


Figure 7. Correlation between physical quantities sensitive to π -electrons conjugation. Panel a: ECC phonon wavenumber vs. ΔE (ΔE is the relative crystal energy - per atom - referred to graphene, see text). Panel b: ΔE vs. BLA parameter. Panel c: ECC phonon wavenumber vs BLA. The data corresponding to 6-h³L crystal are highlighted by a red circle.

Table 5. Sketches of the vibrational eigenvectors associated to the strongest IR active (B_{3u}) phonons of GZY-I, in the spectral region above 2000 cm^{-1} . In the last row the corresponding vibrational frequencies (cm^{-1}) are reported.

6-hL	6-hL ²	6-hL ³	6-L
			
2255 cm^{-1}	2255 cm^{-1}	2256 cm^{-1}	2260 cm^{-1}

Conclusions

The possibility to study how the properties of two dimensional sp - sp^2 carbon materials are affected by the topology and connectivity of sp and sp^2 domains, or by their relative ratio is appealing for

both fundamental and applied research with possible outcomes in technology. Despite the considerable theoretical efforts that have been spent on the assessment of the properties of these materials, most of the current literature focused on the γ polymorph of GDY, or on the α - and β -GDY. Indeed, vibrational properties were analysed only for the γ polymorph [35] and for its nanoribbons [31] whereas a wide range of possible sp - sp^2 carbon materials, in the form of 2D crystals, could constitute interesting alternatives to γ -GDY.

We proposed here a rigorous analysis of the spectroscopic response of different GDY-based 2D crystals. Starting from a previously defined set of structures [52], we have investigated how the Raman active bands (ECC) are affected by different topologies and by the different nature of the sp and sp^2 domains. At the same time, the analysis of the IR spectra gave us the possibility to identify peculiar marker bands able to differentiate between different systems. We started the analysis with the most representative crystals. For these materials, we found a strong dependence of the ECC vibrational frequency on structure, topology and stability. Indeed, the nature of the sp^2 domains strongly influences how the sp linear

chains conjugate with them, strongly modulating the vibrational frequency associated to the ECC mode. Indeed, 6-H presented the most red-shifted ECC frequency while 6-hT² the most blue-shifted. This result is supported by the very nice inter-correlation found between ECC, stability (ΔE) and BLA, which can describe all the physicochemical effects that take place in the analysed 2D crystals.

Similar considerations can be made for the second family, characterized by the presence of both h and L units (named here GZY). Interestingly, by looking at the calculated Raman spectra we can see that the GZY-II series shows a little dispersion of the ECC line, whereas for the GZY-I series the ECC – like phonon shows a dispersion of 130 cm^{-1} , with a decreasing frequency trend as the number of L segments in the L layer increases. This is another proof of the sizeable conjugation effects between the diacetylene segments. Also in this case, the observed trend is supported by the plots correlating ECC, ΔE and BLA. Moreover, the modulation of the ECC phonon frequency is remarkably stronger of GDY (dispersion of about 300 cm^{-1}) than in the whole GZY family (dispersion of 140 cm^{-1}).

These findings are relevant for the possibility to discriminate systems having different structural features, suggesting the application of vibrational spectroscopy for the characterization of topology. Moreover, these results shed light on very peculiar electronic interplay between sp and sp^2 domains that are useful for a proper development of new nanostructured semiconductive sp - sp^2 carbon materials with tailored properties.

Author Contributions

Patrick Serafini: Formal Analysis; Investigation; Writing – original draft; Data Curation; Software

Alberto Milani: Methodology; Software; Data curation; Conceptualization.

Matteo Tommasini: Writing – review & editing; Software; Validation; Data curation

Chiara Castiglioni: Conceptualization; Formal Analysis; Validation; Methodology; Writing – review & editing

Davide M. Proserpio: Conceptualization; Writing – review & editing

Carlo Bottani: Writing – review & editing

Carlo Casari: Supervision; Visualization; Validation; Writing – review & editing; Project administration

Conflicts of interest

There are no conflicts to declare.

Acknowledgements

P.S., A.M., C.C., M.T., C.E.B. and C.S.C. acknowledge funding from the European Research Council (ERC) under the European Union's Horizon 2020 research and innovation program ERC Consolidator Grant (ERC CoG2016 EspLORE grant agreement no. 724610, website: www.esplora.polimi.it).

Notes and references

- 1 A. Hirsch, *Nat. Mater.*, 2010, **9**, 868.
- 2 C. S. Casari, M. Tommasini, R. R. Tykwinski and A. Milani, *Nanoscale*, 2016, **8**, 4414.
- 3 C. S. Casari and A. Milani *MRS Commun*, 2018, **8**, 207.
- 4 A. Milani, A. L. Bassi, V. Russo, M. Tommasini and C. S. Casari *Handbook of Graphene*; Wiley, 2019; Vol. 3.
- 5 A. L. Ivanovskii, *Prog. Solid State Chem.*, 2013, **41**, 1.
- 6 Y. Li, L. Xu, H. Liu, Y. Li, *Chem. Soc. Rev.*, 2014, **43**, 2572.
- 7 N. Zhang, J. Wu, T. Yu, J. Lv, H. Liu and X. Xu, *Front. Phys.*, 2021, **16**, 23201.
- 8 C. Ge, J. Chen, S. Tang, Y. Du and N. Tang, *ACS Appl. Mater. Interfaces* 2019, **11**, 2707.
- 9 X. Gao, H. Liu, D. Wang and J. Zhang, *Chem. Soc. Rev.*, 2019, **48**, 908.
- 10 R. Sakamoto, N. Fukui, H. Maeda, R. Matsuoka, R. Toyoda and H. Nishihara, *Adv. Mater.*, 2019, **31**, 1804211.
- 11 C. Huang, Y. Li, N. Wang, Y. Xue, Z. Zuo, H. Liu and Y. Li, *Chem. Rev.*, 2018, **118**, 7744.
- 12 H. Bao, L. Wang, C. Li and J. Luo, *ACS Appl. Mater. Interfaces*, 2019, **11**, 2717.
- 13 N. Wang, J. He, K. Wang, Y. Zhao, T. Jiu, C. Huang and Y. Li, *Adv. Mater.* 2019, **31**, 1803202.
- 14 C. Xie, N. Wang, X. Li, G. Xu and C. Huang, *Chem. Eur. J.*, 2020, **26**, 569.
- 15 R. H. Baughman, H. Eckhardt and M. Kertesz, *J. Chem. Phys.*, 1987, **87**, 6687.
- 16 E. A. Belenkov, V. V. Mavrinskii, T. E. Belenkova and V. M. Chernov, *J. Exp. Theor. Phys.*, 2015, **120**, 820.
- 17 M. Park, Y. Kim and H. Lee, *npj Comput. Mater.*, 2018, **4**, 541.
- 18 T. Ouyang, C. Cui, X. Shi, C. He, J. Li, C. Zhang, C. Tang and J. Zhong, *Phys. Status Solidi RRL*, 2020, **14**, 2000437.
- 19 E. Belenkov, M. Brzhezinskaya and V. Mavrinskii, *Wiley*, 2019, 113–150.
- 20 P. Yan, T. Ouyang, C. He, J. Li, C. Zhang, C. Tang and J. Zhong, *Nanoscale*, 2021, **13**, 3564.
- 21 D. Malko, C. Neiss, F. Viñes and A. Görling, *Phys. Rev. Lett.*, 2012, **108**, 086804.
- 22 H. J. Cui, X. L. Sheng, Q. B. Yan, Q. R. Zheng and G. Su, *Phys. Chem. Chem. Phys.* 2013, **15**, 8179.
- 23 S. Thomas, H. Li, C. Zhong, M. Matsumoto, W. R. Dichtel and J. L. Bredas, *Chem. Mater.* 2019, **31**, 3051.
- 24 G. Galeotti, F. de Marchi, E. Hamzhepoor, O. MacLean, M. Rajeswara Rao, Y. Chen, L. V. Besteiro, D. Dettmann, L. Ferrari, F. Frezza, P. M. Sheverdyeva, R. Liu, A. K. Kundu, P. Moras, M. Ebrahimi, M. C. Gallagher, F. Rosei, D. F. Perepichka and G. Contini, *Nat. Mater.*, 2020, **19**, 874.
- 25 G. van Miert, C. M. Smith and V. Juričić, *Phys. Rev. B: Condens. Matter Mater. Phys.*, 2014, **90**, 081406.
- 26 G. van Miert, V. Juričić and C. Morais Smith, *Phys. Rev. B: Condens. Matter Mater. Phys.*, 2014, **90**, 195414.
- 27 M. Long, L. Tang, D. Wang, Y. Li and Z. Shuai, *ACS Nano*, 2011, **5**, 2593.
- 28 H. Bai, Y. Zhu, W. Qiao and Y. Huang, *RSC Adv.*, 2011, **1**, 768.
- 29 L. D. Pan, L. Z. Zhang, B. Q. Song, S. X. Du and H. J. Gao, *Appl. Phys. Lett.*, 2011, **98**, 173102.
- 30 H. Bu, M. Zhao, H. Zhang, X. Wang, Y. Xi and Z. Wang, *J. Phys. Chem. A* 2012, **116**, 3934.
- 31 P. Serafini, A. Milani, M. Tommasini, C. Castiglioni and C. S. Casari, *Phys. Rev. Mater.*, 2020, **4**, 014001.
- 32 P. Serafini, A. Milani, M. Tommasini, C. E. Bottani and C. S. Casari, *Carbon* 2021, **180**, 265.
- 33 A. Milani, M. Tommasini, V. Russo, A. Li Bassi, A. Lucotti, F. Cataldo and C. S. Casari, *Beilstein J. Nanotechnol.*, 2015, **6**, 480.
- 34 V. N. Popov and P. Lambin, *Phys. Rev. B*, 2013, **88**, 075427.
- 35 S. Zhang, J. Wang, Z. Li, R. Zhao, L. Tong, Z. Liu, J. Zhang and Z. Liu, *J. Phys. Chem. C*, 2016, **120**, 10605.
- 36 J. Zhao and J. Wang, *J. Phys. Chem. C*, 2017, **121**, 21430.
- 37 J. Wang, S. Zhang, J. Zhou, R. Liu, R. Du, H. Xu, Z. Liu, L. Zhang and Z. Liu, *Phys. Chem. Chem. Phys.*, 2014, **16**, 11303.
- 38 M. M. Haley, *Pure Appl. Chem.*, 2008, **80**, 519.
- 39 J. A. Marsden and M. M. Haley, *J. Org. Chem.*, 2005, **70**, 10213.
- 40 E. L. Spitler, C. A. Johnson and M. M. Haley, *Chem. Rev.*, 2006, **106**, 5344.
- 41 J. A. Marsden, G. J. Palmer and M. M. Haley, *Eur. J. Org. Chem.*, 2003, 2355.
- 42 M. M. Haley, S. C. Brand and J. J. Pak *Angew. Chem., Int. Ed. Engl.*, 1997, **36**, 836.
- 43 W. B. Wan, S. C. Brand, J. J. Pak and M. M. Haley, *Chem. Eur. J.*, 2000, **6**, 2044.
- 44 (44) Kehoe, J. M.; Kiley, J. H.; English, J. J.; Johnson, C. A.; Petersen, R. C.; Haley, M. M. Carbon Networks Based on Dehydrobenzoannulenes. 3. Synthesis of Graphyne Substructures. *Org. Lett.* 2000, **2**, 969–972.
- 45 (45) Diederich, F.; Kivala, M. All-Carbon Scaffolds by Rational Design. *Adv. Mater.* 2010, **22**, 803–812.
- 46 (46) Li, G.; Li, Y.; Liu, H.; Guo, Y.; Li, Y.; Zhu, D. Architecture of Graphdiyne Nanoscale Films. *Chem. Commun.* 2010, **46**, 3256–3258.
- 47 Q. Sun, L. Cai, H. Ma, C. Yuan and W. Xu, *ACS Nano*, 2016, **10**, 7023.
- 48 T. Zhang, Y. Hou, V. Dzhan, Z. Liao, G. Chai, M. Löffler, D. Olanas, A. Milani, S. Xu, M. Tommasini, D. R. T. Zahn, Z. Zheng, E. Zschech, R. Jordan and X. Feng, *Nat. Commun.*, 2018, **9**, 1–11.
- 49 A. Rabia, F. Tumino, A. Milani, V. Russo, A. Li Bassi, S. Achilli, G. Fratesi, G. Onida, N. Manini, Q. Sun, W. Xu, C. S. Casari, *Nanoscale*, 2019, **11**, 18191.
- 50 A. Rabia, F. Tumino, A. Milani, V. Russo, A. L. Bassi, N. Bassi, A. Lucotti, S. Achilli, G. Fratesi, N. Manini, G. Onida, Q. Sun, W. Xu and C. S. Casari, *ACS Appl. Nano Mater.*, 2020, **3**, 12178.
- 51 Q. Sun, R. Zhang, J. Qiu, R. Liu and W. Xu, *Adv. Mater.*, 2018, **30**, 1705630.
- 52 P. Serafini, A. Milani, D. M. Proserpio and C. S. Casari, *J. Phys. Chem. C*, 2021, **125**, 18456
- 53 M. Lorenz, B. Civalleri, L. Maschio, M. Sgroi and D. J. Pullini, *Comput. Chem.*, 2014, **35**, 1789.
- 54 NIST Computational Chemistry Comparison and Benchmark Database NIST Standard Reference Database Number 101 Release 21, August 2020, Editor: Russell D. Johnson III <http://cccbdb.nist.gov/> DOI:10.18434/T47C7Z
- 55 A. Milani, M. Tommasini, M. Del Zoppo, C. Castiglioni, and G. Zerbi, *PHYS. REV. B*, 2006, **74**, 153418
- 56 F. Innocenti, A. Milani and C. Castiglioni, *J. Raman Spectrosc.*, 2010, **41**, 226
- 57 A. Lucotti, M. Tommasini, D. Fazzi, M. Del Zoppo, W. A. Chalifoux, M. J. Ferguson, G. Zerbi and R. R. Tykwinski, *J. Am. Chem. Soc.* 2009, **131**, 4239
- 58 M. Tommasini, D. Fazzi, A. Milani, M. Del Zoppo, C. Castiglioni and G. Zerbi, *J. Phys. Chem. A* 2007, **111**, 11645
- 59 S. Kamalinahad, F. Viñes and P. Gamallo, *J. Phys. Chem. C*, 2019, **123**, 27140.